Excited-state absorption mechanisms in red-laser-pumped uv and blue upconversions in Tm^{3+}-doped fluoroaluminate glass

S. Tanabe
Department of Chemistry, College of Liberal Arts and Sciences, Kyoto University, Sakyo-ku, Kyoto 606-01, Japan

K. Tamai, K. Hirao, and N. Soga
Department of Industrial Chemistry, Faculty of Engineering, Kyoto University, Sakyo-ku, Kyoto 606-01, Japan
(Received 14 January 1992)

The mechanism of red-pumped frequency-upconversion fluorescence observed in the uv and blue ranges of frequencies for a Tm^{3+}-doped fluoroaluminate glass was investigated by single-wavelength pumping of a tunable 4-(dicyanomethylene)-2-methyl-6-(*p*-dimethyl-amino-styryl)-4*H*-pyran dye laser. It was found that the dependences of fluorescence intensity on the incident excitation power were quadratic both for the 0.36- and 0.45-μm emissions, which originate from $^1D_2$, and for the 0.48-μm emission from $^1G_4$, indicating two-step excitation mechanisms. The excitation profile for the normal emission varied in the same way as that of the ground-state absorption spectra of the $^3F_4 \leftarrow {}^3H_6$ transition, while those for upconversion emissions shifted to the higher-energy side. Moreover, the excitation process to the $^1G_4$ level was found to be different from that to the $^1D_2$ level. It was concluded that the mechanisms leading to these upconversion emissions are excited-state absorption (ESA) for both levels and that the process to the $^1D_2$ level is ESA from $^3F_4$, while that to the $^1G_4$ level is from the $^3F_4$ level after nonradiative decay from the upper levels. The results were discussed in terms of the slow multiphonon decay rate from the $^1D_2$ to the $^1G_4$ level in this glass.

I. INTRODUCTION

A blue-emitting laser is an attractive material because there is a need for higher density in optical data storage as well as for multicolorization of visible lasers. Frequency upconversion of rare-earth doped glasses has the possibility of producing infrared-pumped visible lasers with use of a III-V semiconductor laser. For example, Er^{3+} ions can efficiently convert infrared radiations of widely used laser diodes ($\lambda = 1.5$, 0.98, 0.80 μm) into green emission around 0.55 μm.[1-3] However, it has been difficult to obtain blue emission by Er^{3+} and Ho^{3+}.[4] On the other hand, Tm^{3+} ions have stable excited levels emitting blue fluorescence ($^1D_2$, $^1G_4$). Fluoride glasses can be considered as candidate materials for Tm^{3+} blue upconversion lasers, since the nonradiative loss due to multiphonon relaxation is suppressed by their lower phonon energy.[5] Recently, blue upconversion lasing was obtained in a fluorozirconate glass fiber by co-pumping at 676.4 and 647.1 nm using a krypton-ion laser.[6] Monerie *et al.*[7] obtained evidence of the excited-state absorption (ESA) mechanisms of Tm^{3+} upconversion in their investigation of the power dependence of the absorption parameters of fluoride fibers. Although these pumping wavelengths are not in the infrared region but rather in the visible red, pumping laser sources around 0.65 μm became available with the development of Al-Ga-In-P semiconductor lasers with quantum-well structures.[8] To design an efficient frequency upconverter, it is also important to get direct evidence of the upconversion mechanisms in the glass. In this study, the Tm^{3+} upconversion characteristics were investigated by single-wavelength pumping of a tunable laser around 0.65 μm. Generally, for the upconversion by the energy transfer [photon addition by energy transfer (PAET)] mechanisms, the incident light is absorbed only in transitions from the ground state and the energy transfer occurs between adjacent excited ions. Thus the wavelength dependence of upconversion efficiency should vary only with the ground-state absorption profile.[9] In the case of ESA mechanisms, the efficiency depends on both the ground-state and excited-state absorptions. The ESA cross section is usually expected to vary with wavelength in the same way as the ground-state absorption. Therefore, the excitation spectra[9] were monitored by tuning across the Tm^{3+}:$^3F_{2,3} \leftarrow {}^3H_6$ absorption profile with a 4-(dicyanomethylene)-2-methyl-6-(*p*-dimethyl-amino-styryl)- 4*H*-pyran (DCM) dye laser source and the excitation process leading to upconversion was discussed.

II. EXPERIMENT

Glass in the composition 40.5% AlF_3-21.8% CaF_2-21.8% BaF_2-14.9% YF_3-1% TmF_3 was prepared by using reagent grade AlF_3, CaF_2, BaF_2, YF_3, and TmF_3. A small amount of $NH_4F \cdot HF$ was also added to complete the fluorination. The powders of batch composition were well mixed in an alumina mortar and melted in a platinum crucible at 1000 °C for 15 min. The melt was poured on stainless steel and pressed with a stainless-steel plate. The glass obtained was annealed at 435 °C for 15 min and cut into $4 \times 4 \times 1$ mm^3 size and polished with diamond paste. The density was measured by the Archimedes method to calculate the number of Tm^{3+} ions per unit volume, ρ_N, with the molar weight. The refractive index n_D was measured with an Abbe refractom-

eter. The absorption spectrum was measured with a Shimadzu UV-3101PC recording spectrophotometer in the wavelength range 200–2000 nm. From the integrated absorbance, three intensity parameters Ω_t (t = 2,4,6), which identify the ligand field and dominate the transition probabilities in the glass, were determined as follows: since the line strength S for electric-dipole transitions between an initial $|aJ\rangle$ and final $|bJ'\rangle$ manifold is given by[10,11]

$$S(aJ;bJ')=\sum_{t=2,4,6}\Omega_t\langle aJ||U^{(t)}||bJ'\rangle^2 , \quad (1)$$

where $\langle aJ||U^t||bJ'\rangle^2$ denote the reduced matrix elements of unit tensor operators for the corresponding transition, a least-squares fitting approach was done by using ρ_N, n_D, and the integrated absorbance of five bands listed in Table I. Fluorescence spectra were recorded with a Hitachi-850 fluorescence spectrophotometer. As an excitation source, a dye laser apparatus (Spectra Physics model 375 dye laser) excited by an Ar^+ laser (Coherent Innova 70) was used with the propylene carbonate solution of DCM dye, having the emission wavelength range 630–700 nm, which correspond to the Tm^{3+}:$^3F_{2,3}\leftarrow{}^3H_6$ ground-state absorption. The beam area of the dye laser was 1 mm^2 in the glass sample. The excitation wavelength was tuned with a tuning wedge and the power was controlled by an Ar^+ laser and determined by a power meter (Coherent 210 power meter). The maximum flux density of 0.65 μm radiation obtained was 360 mW/mm^2.

III. RESULTS

The absorption spectrum of the fluoroaluminate glass is shown in Fig. 1. Each assignment in Fig. 1 corresponds to the upper level of the transition from the ground $^3H_6$ state. With the obtained line strengths of five bands listed in Table I, a least-squares fitting approach was done with use of the values $\rho_N=1.698\times10^{20}$ cm^{-3} and $n_D=1.432$. The measured and calculated line strengths are listed in Table II. The obtained parameters were $\Omega_2=1.75\times10^{-20}$ cm^2, $\Omega_4=1.33\times10^{-20}$ cm^2, and $\Omega_6=1.27\times10^{-20}$ cm^2. The root mean square deviation was only 0.20%, indicating a good fit.

An efficient upconversion could be obtained around 0.655 μm by excitation. The fluorescence spectrum with

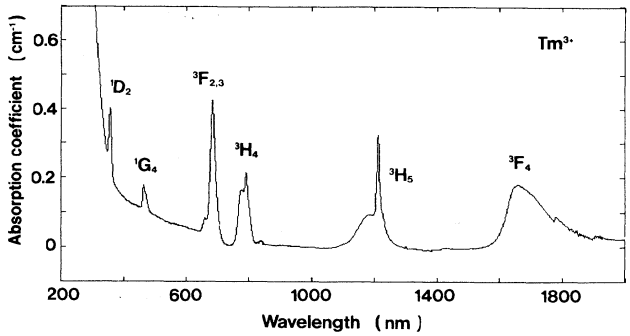

FIG. 1. Absorption spectrum of glass.

0.655 μm excitation is shown in Fig. 2 for various pumping powers. The largest peak overscaled is due to the Rayleigh scattering of the incident pump light. Upconversion fluorescences peaking at 363, 451, 476 nm, and the one-step fluorescence at 793 nm would be seen. The blue emissions at 451 and 476 nm could be clearly detected by human eyes with pumping powers less than 100 mW. The power dependence of emission intensity on the incident pumping power is plotted in Fig. 3. The 793 nm emission clearly shows a linear dependence against pumping power while other emissions show nonlinear dependences.

The variation of fluorescence spectra with the excitation wavelength is shown in Fig. 4. The excitation power was fixed at 100 mW. Figure 4 shows that the intensities of the upconversion fluorescence at uv and blue region increased up to around the 650 nm excitation and decreased with an increase of the excitation wavelength. On the other hand, the intensity of the one-step fluorescence around 790 nm increased with an increase of the excitation wavelength and showed a maximum around the 682 nm excitation.

IV. DISCUSSION

A. Fluorescence spectra of Tm^{3+} in glass

In the present fluoride glass, the apparent branching ratio of the 360 nm emission is comparable to that of the 450 nm emission. In the fluorescence spectra of Tm^{3+}-

TABLE I. $\langle SLJ||U^t||S'L'J'\rangle$ for f^{12} from Ref. 12.

SLJ	$S'L'J'$	$\langle U^2\rangle^2$	$\langle U^4\rangle^2$	$\langle U^6\rangle^2$	λ (μm)	Band
$^3H_6$	$^3F_4$	0.5589	0.7462	0.2574	1.7	1
	$^3H_5$ [a]	0.1074	0.2313	0.6382	1.2	
	$^3H_4$	0.2187	0.0944	0.5758	0.79	2
	$^3F_3$	0.0	0.3163	0.8409	0.68	3
	$^3F_2$	0.0	0.0000	0.2591	0.65	
	$^1G_4$	0.0452	0.0694	0.0122	0.47	4
	$^1D_2$	0.0	0.3133	0.0934	0.36	5

[a] Including magnetic dipole contribution.

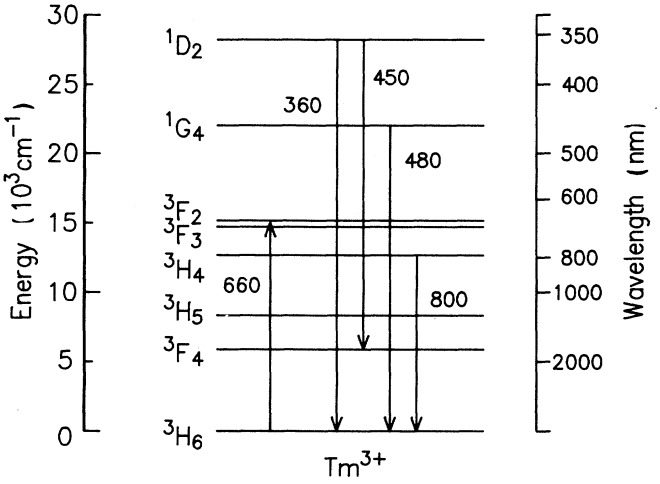

FIG. 2. Energy levels of the Tm^{3+} ion.

doped silica fibers reported by Hanna *et al.*,[13] the emission around 460–470 nm was observed, but the emission peak from the $^1D_2$ level and that from the $^1G_4$ level were not well resolved. It is presumably due to the large Stark splitting and inhomogeneous broadening, as well as energy shifts of these levels in the oxide host. On the other hand, in the fluoride host in this study the emissions at 451 nm due to the $^1D_2 \rightarrow {}^3F_4$ transition and at 476 nm due to the $^1G_4 \rightarrow {}^3H_6$ transition is clearly resolved. In addition to the blue emissions, the 360 nm emission in the uv range is clearly observed, which is due to the $^1D_2 \rightarrow {}^3H_6$. The relative intensity of this uv emission was larger compared with the spectrum of the doped silica glass,[13] in which the peak around 370 nm is only weakly detected. This is ascribed to the different branching ratio β from the $^1D_2$ level, owing to the different ratio of spontaneous emission probabilities, A. The branching ratio β

TABLE II. Measured and calculated line strengths for five bands of Tm^{3+} in the glass.

Band	λ (nm)	$S(10^{-20}$ cm$^2)$	$S_c(10^{-20}$ cm$^2)$
1	1696	2.288	2.295
2	785.6	1.236	1.238
3	684.6	1.816	1.813
4	467.1	0.281	0.187
5	356.4	0.521	0.534

$\Omega_2 = 1.75\times10^{-20}$ cm^2
$\Omega_4 = 1.33\times10^{-20}$ cm^2
$\Omega_6 = 1.27\times10^{-20}$ cm^2 $\delta_{rms}=0.20\%$

from the $|aJ\rangle$ state may be defined as

$$\beta(aJ;bJ')=\frac{A(aJ;bJ')}{\sum_{bJ'} A(aJ;bJ')} . \quad (2)$$

where the denominator is the summation to all lower terminal states $|bJ'\rangle$. Thus the factors dominating the branching ratio from the $^1D_2$ to the lower states are the relative values of A, which are the functions of reduced matrix elements of each transition and also a set of Ω_t intensity parameters of a given ligand field. Here, the spontaneous emission probability A for electric-dipole transitions is given by[10,11]

$$A(aJ;bJ')=\frac{64\pi^2e^2}{3h(2J+1)}\frac{1}{\lambda^3}\frac{n(n^2+2)^2}{9}S(aJ;bJ') , \quad (3)$$

where $S(aJ;bJ')$ is defined by Eq. (1) in Sec. IV A.

Table III shows the sets of $\langle||U^t||\rangle^2$ for all the possible radiative transitions from the $^1D_2$ level.[12] As seen from Table III, the $\langle||U^2||\rangle^2$ for the $^1D_2 \rightarrow {}^3H_6$ transition is 0, while that for the $^1D_2 \rightarrow {}^3F_4$ transition is

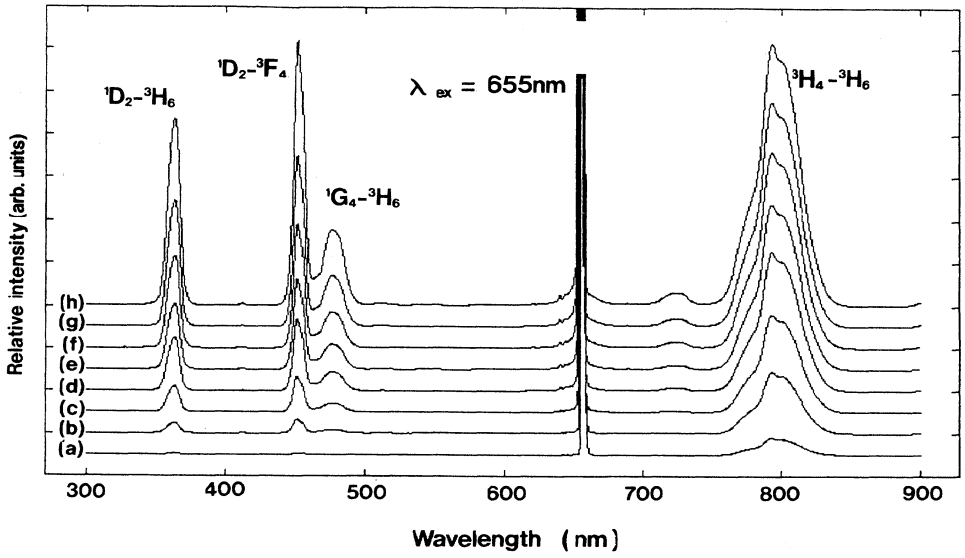

FIG. 3. Emission spectra of glass pumped by 0.655 μm with the power of (a) 20 mW, (b) 60 mW, (c) 100 mW, (d) 150 mW, (e) 200 mW, (f) 250 mW, (g) 300 mW, and (h) 360 mW.

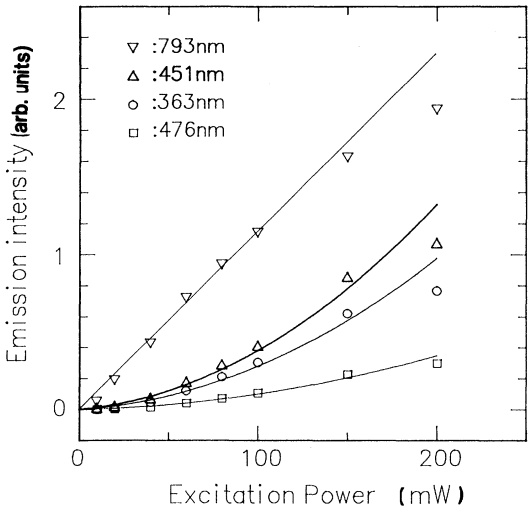

FIG. 4. Dependence of the emission intensity on the 0.655 μm pumping power.

nonzero and large. Since the values of $\langle||U^t||\rangle^2$ for the transitions to terminal states other than $^3H_6$ and $^3F_4$ are negligibly small, the branching ratio of 0.36 μm emission, $\beta(^1D_2;^3H_6)$, is dominated by the value of Ω_2 and Ω_4.

From Eqs. (2) and (3), and Table III, the branching ratios of the 360 and 450 nm emissions in the present glass were calculated with the Ω_t values to find 0.40 and 0.45, respectively (Table IV). This result is in accord with the observed fluorescence spectra in Fig. 3. Since the $\langle||U^2||\rangle^2$ of the $^1D_2 \rightarrow {}^3F_4$ transition is large, the branching ratio β of the blue emission would be largely enhanced by the higher value of Ω_2, which reflects the asymmetry of the ligand field.[14,15] As is often observed for most glass systems, the values of Ω_2 rare-earth ions in oxide glasses are larger than those in fluoride glasses.[16] This is ascribed to the larger electric-field gradient by divalent oxide ions than by monovalent fluoride ions and also due to the effect of covalency of the chemical bond between rare earth and ligand anions. On the other hand, the values of $\Omega_{4,6}$ are not so strongly sensitive to changes of the host composition.[15] Therefore, the branching ratio β of the transitions with a large $\langle||U^4||\rangle^2$ is relatively enhanced in fluoride hosts where Ω_2 is small. That is the reason for the higher β value of the $^1D_2 \rightarrow {}^3H_6$ transition up to $\beta = 40\%$ in the fluoride host with a smaller Ω_2 value.

B. Pumping power dependence of fluorescence intensity

As seen in Fig. 2, the intensity of the upconversion emission increased dramatically with increasing excitation power, while the intensity at 793 nm increased linearly. At higher pumping powers, the intensity of upconversion fluorescence is comparable to that of one-step fluorescence. The nonlinear power dependence of emission intensities in the uv and blue regions on the incident pumping power in Fig. 3 indicates multistep excitation. A log-log plot is shown in Fig. 5. Each slope corresponds to the number of steps needed for the excitation, although there seems to be the effect of saturation at higher pumping power. This saturation is probably due to the depopulation of the ground level. Therefore, both the uv and blue emissions occur by a two-step process with 0.65 μm excitation in this fluoride glass.

C. Wavelength dependence of fluorescence intensity

As seen in Fig. 4, the suitable pumping wavelengths for upconversion fluorescences were different from that for one-step fluorescence. The laser excitation spectra for each emission are plotted in Fig. 6. It can be seen that the excitation efficiency of the 793 nm fluorescence shows a maximum around 683 nm, while those of three upconversion fluorescences shift to a higher energy side. The former profile is almost the same as that of the ground-state absorption ($^3F_{2,3} \leftarrow {}^3H_6$) spectrum, which is shown in Fig. 7. This is due to the fact that the emission from the $^3H_4$ level occurs after the multiphonon relaxation from the $^3F_{2,3}$ level. On the other hand, the three upconversion profiles are different from the ground-state absorption (GSA) profile. These results can be ascribed to the presence of ESA mechanisms and not PAET for the upconversion emissions. It is obvious that the Tm^{3+} is first promoted to the $^3F_{2,3}$ level and then is raised from a certain lower intermediate level to a still higher state by the second-step excitation. To reach the $^1D_2$ level with aid of the second incident photon, the $^3H_4$ level, which is $\sim 1800\ cm^{-1}$ below the $^3F_3$ level, is taken to be the intermediate level from which ESA occurs. The efficient wavelength for the $^1D_2 \leftarrow {}^3H_4$ absorption was estimated from the absorption spectrum and found to be about 650 nm. It is reasonable that the excitation profiles of 360

TABLE III. Reduced matrix elements $\langle(SL)J||U^t||(S'L')J'\rangle^2$ of radiative transitions from the $^1D_2$ level of Tm^{3+}.[12] Typical wavelengths are included.

$(SL)J$	$(S'L')J'$	$[U^2]^2$	$[U^4]^2$	$[U^6]^2$	λ (μm)
$^1D_2$	$^3H_6$	0.0	0.3133	0.0934	0.36
	$^3F_4$	0.5792	0.0968	0.0194	0.45
	$^3H_5$	0.0	0.0017	0.0164	0.50
	$^3H_4$	0.1147	0.0138	0.2307	0.65
	$^3F_3$	0.1637	0.0714	0.0	0.76
	$^3F_2$	0.0639	0.3093	0.0	0.80
	$^1G_4$	0.1926	0.1666	0.0006	1.8

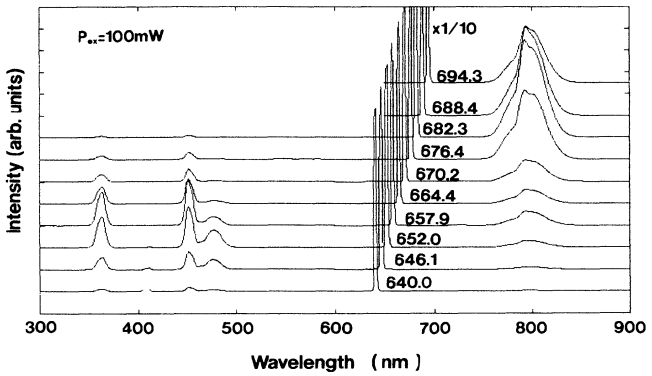

FIG. 5. Variation of fluorescence spectra with pumping wavelength. The pumping wavelength is shown in nm scale and the power is fixed at 100 mW.

and 450 nm are equivalent, except that their intensity ratios were determined only by the branching ratio β from the $^1D_2$ level. Because of the absence of higher final levels with a suitable energy for ESA by a two-step process, the main mechanism leading to the upconversion of $^1D_2 \rightarrow {}^3H_6, {}^3F_4$ transitions can be taken to be the ESA from the $^3H_4$ to the $^1D_2$ level. The energy gap between the $^3H_4$ and the next lower level is large enough to maintain a long lifetime in this fluoride host with a phonon energy of 600 cm^{-1}, which is ascribed to the Al-F stretching vibration in the glass.[16] The wavelength of 655 nm at maximum in Fig. 6 is placed between that of ESA and GSA of Tm^{3+}. A small shift of the peak to a lower energy side than that of ESA can be due to the contribution of GSA efficiency, which shows a maximum at 682 nm in Figs. 6 and 7. In this glass, the upconversion is attained

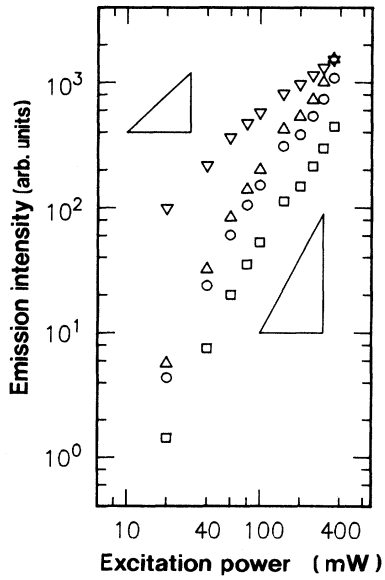

FIG. 6. The log-log plot of the emission intensity and pumping power. ∇: 793 nm, △: 451 nm, ○: 363 nm, and □: 476 nm. The triangles indicate the slope of 2 and 1.

TABLE IV. Spontaneous emission probability A and branching ratio β of radiative transitions from the $^1D_2$ level of Tm^{3+} in the glass.

$(SL)J$	$(S'L')J'$	A (s^{-1})	β
$^1D_2$	$^3H_6$	4586	0.40
	$^3F_4$	5119	0.45
	$^3H_5$	74	0.01
	$^3H_4$	745	0.07
	$^3F_3$	347	0.03
	$^3F_2$	408	0.04
	$^1G_4$	38	0.00

by single-wavelength pumping, owing to the overlapping of these two absorption energy ranges around 655 nm.

Figure 8 shows the upconversion fluorescences for various pumping wavelengths. Apparently, the emission intensity from the $^1G_4$ level varies differently. This is not the effect of the fluorescence line narrowing for different sites in amorphous states, which could be observed for transitions involving the level with a singlet J state ($J=0,1/2$), such as Eu^{3+}:$^5D_0$[17] or at most, a doublet J state ($J=3/2$), such as Nd^{3+}:$^4F_{3/2}$ at low temperatures,[18] by using lasers with a much narrower spectral width (~ 0.3 cm^{-1}). Thus, in the case of the $^1G_4 \rightarrow {}^3H_6$ fluorescence at 476 nm, other mechanisms can contribute to that of $^1D_2$ emissions because the excitation profile ob-

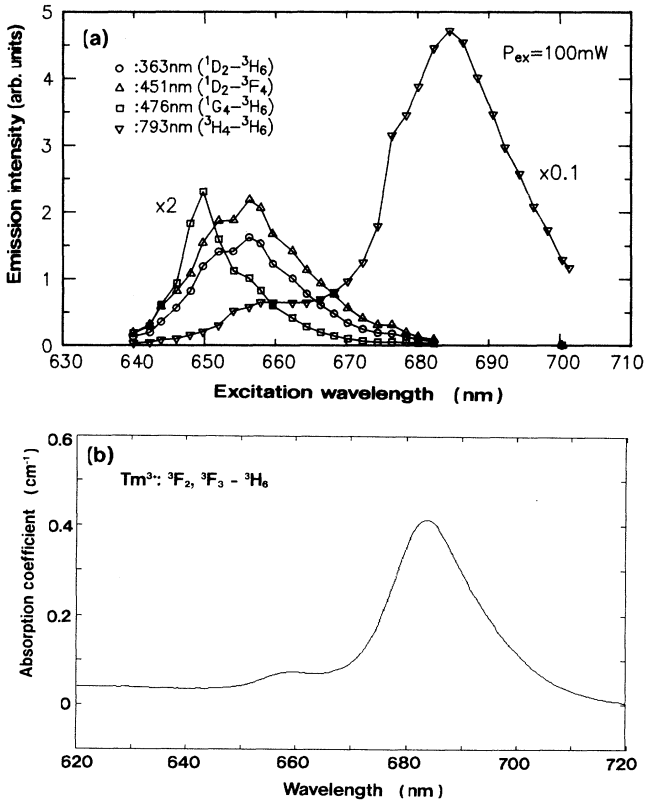

FIG. 7. (a) Emission intensities as a function of excitation wavelength. (b) Absorption spectrum of Tm^{3+}:$^4F_{2,3} \leftarrow {}^3H_6$ transition in the glass.

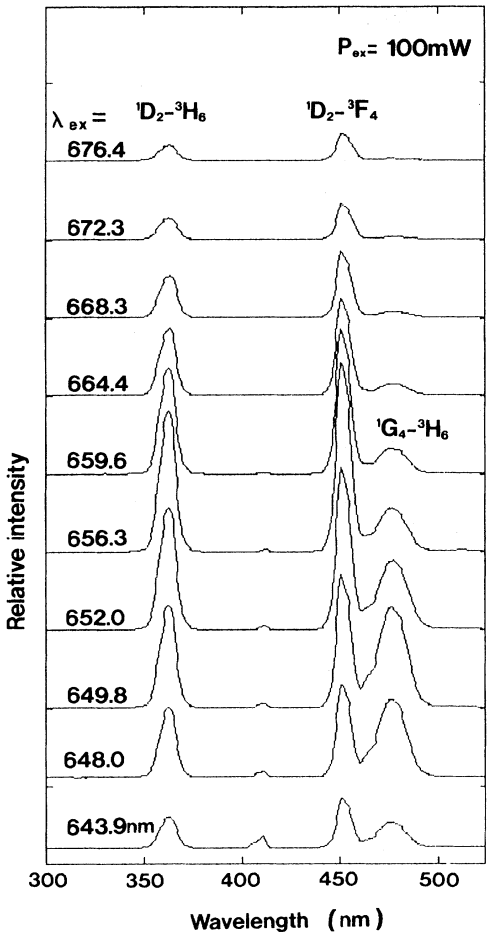

FIG. 8. Variation of upconversion spectra with different pumping wavelengths, λ_{ex}. The λ_{ex} is shown in each spectrum.

served in Fig. 6 is different. One possible mechanism involves the $^3F_4$ level, which is populated after multiphonon decay from the $^3H_4$ level and pumped with a second incident photon with about 645 nm to the $^1G_4$ level. A larger energy difference of the $^1G_4 \leftarrow {}^3F_4$ ESA transition from GSA can be the reason for the shift of the excitation profile of $^1G_4$ emission to a higher energy side than that of the $^1D_2$ level. Another possible mechanism is the same ESA as $^1D_2$ followed by multiphonon decay $^1D_2 \Longrightarrow {}^1G_4$. This latter process seems plausible in view of the small overlapping of both profiles around 655 nm in Fig. 6. In order to confirm the possibility of multiphonon decay, the fluorescence and excitation spectra were measured.

Shown in Figs. 9(a) and 9(b) are the fluorescence spectra by the laser (λ=650 nm) and Xe-lamp (λ= 352 nm) excitations, respectively. The peak around 476 nm is clearly observed in (a), whereas it is scarcely seen in (b), and moreover, the emission from the $^3H_4$ level around 790 nm is quite weak. Both results indicate that the multiphonon decay rate from the $^1D_2$ to the next lower level is too small to populate the $^1G_4$ level as also shown for the Tm^{3+}:$YLiF_4$ crystal[19] and still lower levels such as $^3H_4$. This is supported by the excitation results in Figs. 9(c) and 9(d), that uv excitation around 350 nm is responsible for the 451 nm emission but not for the 473 nm emission. Accordingly, the contribution of the second mechanism is negligibly small and the ESA from the $^3F_4$ level is responsible for the upconversion from the $^1G_4$ level.

D. Contribution of nonradiative decay process to upconversion mechanisms

In the preceding section C, the multiphonon relaxation (MPR) rate at the $^1D_2 \Longrightarrow {}^1G_4$ transition was found to be negligibly slow in this fluoride host. However, it would be impossible to observe $^1G_4$ upconversion by the proposed mechanism, if the nonradiative decay did not occur from the $^3F_{2,3}$ and $^3H_4$ levels to the $^3F_4$ level. To check both mechanisms, the MPR rate, $W_p(T)$ was calculated for the levels of Tm^{3+} ion by the following equations:[20]

$$W_p(T)=W_0(0)\exp(-\alpha\Delta E/\hbar\omega)\ , \tag{4}$$

$$\alpha=\ln\{p/g[n(T)+1]\}-1\ , \tag{5}$$

$$p\simeq\Delta E/\hbar\omega\ , \tag{6}$$

where ΔE is the energy gap to the next lower level, g is the electron-phonon coupling strength, p is the phonon number consumed during MPR, and $W_0(0)$ is the decay

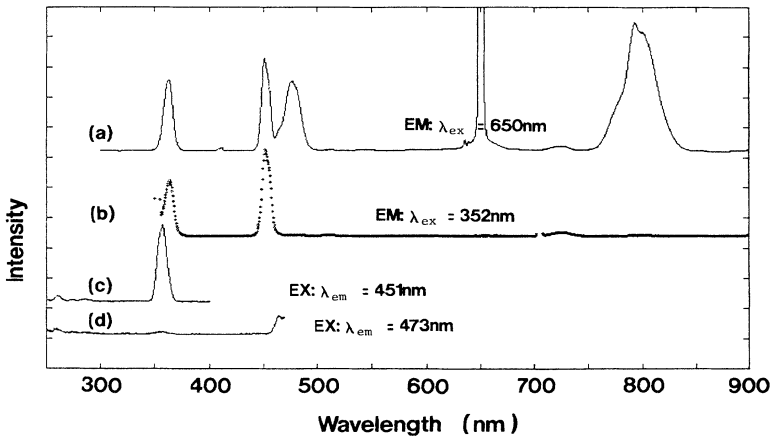

FIG. 9. Emission and excitation spectra of blue emissions: (a) emission spectrum by 650 nm excitation, (b) emission spectrum by 352 nm excitation, (c) excitation spectrum of 451 nm emission, and (d) excitation spectrum of 473 nm emission.

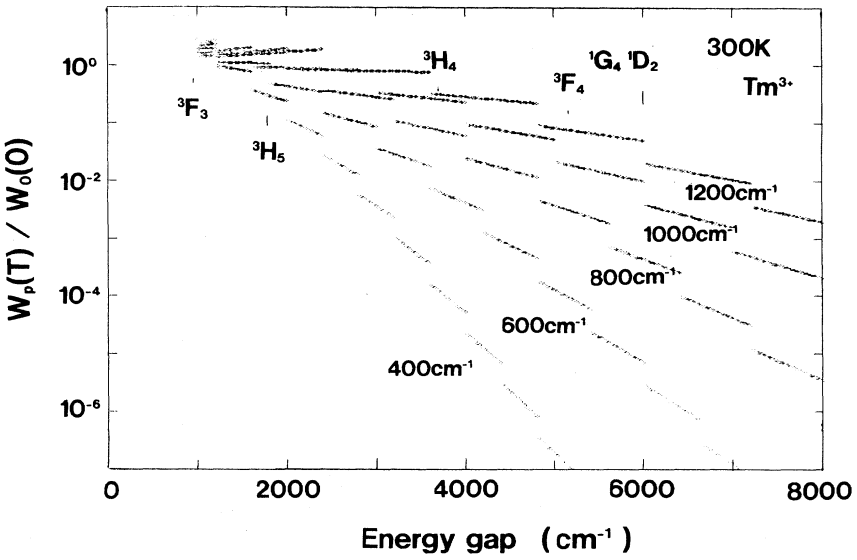

FIG. 10. Multiphonon decay rate as a function of the energy gap for various phonon energies. The corresponding Tm^{3+} levels are indicated.

rate at $\Delta E=0$ and $T=0$. The temperature dependence of W_p arises from its dependence upon the Planck distribution function, $n(T)$[21] on the occupation number of the phonon mode;

$$n(T) = [\exp(\hbar\omega/kT)-1]^{-1} . \quad (7)$$

In the calculation, only integer values for the number of phonons p and a temperature-independent constant value of g were used. In Fig. 10 the ΔE dependences of W_p(300 K) are plotted for various phonon energies. Apparently, W_p decreases with increasing ΔE and decreasing $\hbar\omega$. Since g depends on the structure or lattice nature of the host but not on the electronic nature of each wave function,[22] it is possible to compare the relative W_p for excited states of Tm^{3+} with various ΔE in this glass. It can be seen that W_p for the $^1D_2$, $^1G_4$, and $^3F_4$ levels are much lower by a few orders of magnitude, for which much longer lifetimes are expected than those for $^3F_3$ and $^3H_5$ levels, where the electrons are to decay rapidly to the $^3H_4$ and $^3F_4$ levels, respectively. This tendency is more pronounced for the lower phonon energy, i.e., also in the present fluoride glass ($\hbar\omega$ = 600 cm^{-1}). Accordingly, the nonradiative lifetime of the $^1D_2$, $^1G_4$, and $^3F_4$ levels can be increased effectively with decreasing phonon energy of the host. The latter two levels play a dominating role as an emitting or intermediate state on the upconversion efficiency of the $^1G_4 \rightarrow {}^3H_6$ emission. On the efficiency of $^1D_2$ upconversions, the lifetime of the $^3H_4$ level also becomes a dominating factor as an intermediate state. Although the W_p of the $^3H_4$ level is lower than that of the $^3F_3$ level, it is still higher than that of the $^3F_4$ level. As a consequence, the following ordering is expected for the nonradiative lifetimes, $^3F_3 < {}^3H_5 \ll {}^3H_4 \ll {}^3F_4 < {}^1G_4 \simeq {}^1D_2$. Thus the lifetime of the $^3F_4$ level can be found between them. From the discussion in Sec. C and the calculated W_p, the quantum efficiency of the $^1D_2$ level is considered to be almost unity, whereas those of the $^3F_3$ and $^3H_5$ levels are almost zero. The lifetime of the $^3H_4$ level dominates the ratio of total electronic transition rate (including ESA) to the nonradiative decay rate. This ratio is responsible for the intensity ratio of upconversion emissions from the $^1D_2$ and $^1G_4$ levels, to which ESA's occur from the $^3H_4$ and $^3F_4$ levels, respectively. Because both emissions are observed by suitable pumping conditions, the quantum efficiency of the $^3H_4$ level cannot be near zero nor unity. For this reason, it is possible to change the ratio of 450 to 480 nm emission intensities, by controlling the W_p of the $^3H_4$ level (Fig. 11) as well as by tuning the pumping wavelength.

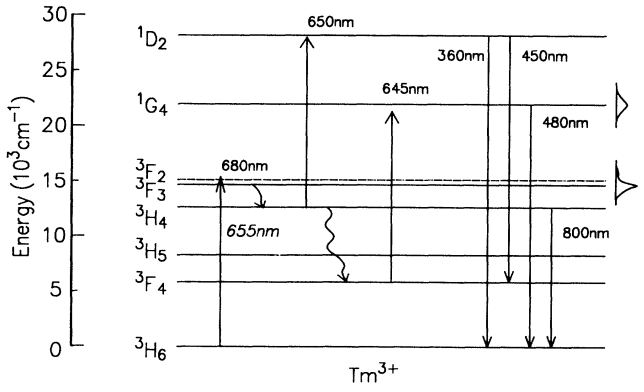

FIG. 11. Upconversion mechanism of this glass.

V. CONCLUSIONS

In conclusion, evidence is given of the excited-state absorption mechanisms of uv and blue-upconversion fluorescences in Tm^{3+}-doped fluoride glass with use of a

tunable DCM dye laser for single-wavelength pumping. The process leading to the $^1D_2$ level for the 0.36 and 0.45 μm emissions was found to be different from that to the $^1G_4$ level for the 0.48 μm emission. The transitions $^1D_2 \leftarrow {}^3H_4$ and $^1G_4 \leftarrow {}^3F_4$ are the corresponding ESA. It was concluded that the multiphonon decay rate from the $^1D_2$ to the $^1G_4$ level was very low in this glass, with a phonon energy of 600 cm^{-1}.

[1]J. P. van der Ziel, L. G. Van Uitert, W. H. Grokiewicz, and R. M. Mikulyak, J. Appl. Phys. **60**, 4262 (1986).

[2]D. C. Yeh, W. A. Sibley, M. Suscavage, and M. G. Drexhage, J. Appl. Phys. **62**, 266 (1987).

[3]S. Tanabe, K. Hirao, and N. Soga, J. Non-Cryst. Solids **122**, 79 (1990).

[4]J. Y. Allain, M. Monerie, and H. Poignant, Electron. Lett. **26**, 261 (1990).

[5]C. B. Layne and M. J. Weber, Phys. Rev. B **16**, 3259 (1977).

[6]J. Y. Allain, M. Monerie, and H. Poignant, Electron. Lett. **26**, 166 (1990).

[7]M. Monerie, T. Georges, P. L. Francois, J. Y. Allain, and D. Neveux, Electron. Lett. **26**, 320 (1990).

[8]M. Ikeda, A. Toda, K. Nakano, Y. Mori, and N. Watanabe, Appl. Phys. Lett. **50**, 1033 (1987).

[9]S. Tanabe, S. Yoshii, K. Hirao, and N. Soga, in *Science and Technology of New Glasses,* edited by S. Sakka and N. Soga (Ceramic Society of Japan, Tokyo, 1991), p. 193.

[10]B. R. Judd, Phys. Rev. **127**, 750 (1962).

[11]G. S. Ofelt, J. Chem. Phys. **37**, 511 (1962).

[12]N. Spector, R. Reisfeld, and L. Boehm, Chem. Phys. Lett. **49**, 49 (1977).

[13]D. C. Hanna, R. M. Percival, I. R. Perry, R. G. Smart, J. E. Townsend, and A. C. Tropper, Opt. Commun. **78**, 187 (1990).

[14]C. K. Jørgensen and B. R. Judd, Mol. Phys. **8**, 281 (1964).

[15]S. Tanabe, T. Ohyagi, N. Soga, and T. Hanada, Phys. Rev. B **46**, 3305 (1992).

[16]S. Tanabe, K. Hirao, and N. Soga, J. Non-Cryst. Solids **142**, 148 (1992).

[17]J. R. Morgan, E. P. Chock, H. D. Hopewell, M. A. El-Sayed, and R. Orbach, J. Phys. Chem. **85**, 747 (1981).

[18]J. M. Pellegrino, W. M. Yen, and M. J. Weber, J. Appl. Phys. **51**, 6332 (1980).

[19]M. Dulick, G. E. Faulkner, N. J. Cockroft, and D. C. Nguyen, J. Lumin. **48&49**, 517 (1991).

[20]T. Miyakawa and D. L. Dexter, Phys. Rev. B **1**, 2961 (1970).

[21]C. Kittel, *Introduction to Solid State Physics,* 6th ed. (Wiley, New York, 1986), p. 101.

[22]C. B. Layne, W. H. Lowdermilk, and M. J. Weber, Phys. Rev. B **16**, 10 (1977).